Design Improvement and Bias Voltage Optimization of Glass-Body Microchannel Plate Picosecond Photodetector

Jingbo Wang, Karen Byrum, Marcel Demarteau, Ranjan Dharmapalan, Jeffrey W. Elam, Anil U. Mane, Edward May, Robert Wagner, Dean Walters, Junqi Xie, Lei Xia, and Huyue Zhao

***Abstract*— Microchannel plate photodetectors, capable of picosecond time resolution and sub-mm spatial resolution, are a perfect candidate for the next generation of photodetectors for precision timing measurements. Argonne National Laboratory is producing low-cost, all-glass body, planar photodetectors with an indium seal. The design and fabrication of 6-cm square photodetectors has been well demonstrated in an ultra-high vacuum system. Recently, a new design was developed to optimize the photodetector bias voltage. This design offers an improved configuration and allows external control of the bias voltage for each internal detector component. Design and measurements of the new independently biased devices are described in this paper. We performed a systematic study on the bias voltage and achieved a gain on the order of 10^7, a time resolution better than 35 ps, and a spatial resolution better than 1 mm.**

***Index Terms*— Bias voltage, gain, microchannel plate, optimization, photodetector, spatial resolution, time resolution.**

I. Introduction

FOR decades, photomultiplier tubes (PMTs) [1] have been widely used by nuclear and particle physics experiments for building a wide variety of detector systems that require weak light detection and large scale coverage. Traditional PMTs have high gain, high quantum efficiency, good time resolution and sensitivity to single photons. However, the discrete dynode structure limits their positioning capability. In addition, their performance under high magnetic field is still an issue. Increasingly, the nuclear and particle physics community has called for a next generation of photodetectors with capabilities better than those of traditional PMTs [2].

Microchannel plate (MCP) photodetectors [3] are compact photon sensors simultaneously providing picosecond level time resolution and sub-mm level spatial resolution, which makes them a promising candidate for the replacement of traditional PMTs. MCP photodetectors offer a high electron gain that allows single photon detection. In addition, MCP photodetectors have shown potential in withstanding high magnetic fields. However, the conventional fabrication method of MCP photodetectors is too expensive for building large-area systems, such as Ring-Imaging Cherenkov (RICH) detectors for collider or neutrino experiments. The large-area picosecond photodetectors (LAPPD) collaboration [4] was formed in 2009. One of the goals of the LAPPD collaboration was to develop new, commercializable methods to fabricate large-area photodetectors at a reduced cost with the capability of fast timing (<10 ps). Recent advances in the fabrication of the MCPs using borosilicate glass capillary arrays which have been functionalized through the atomic layer deposition (ALD) technique offer an opportunity of producing next generation low cost photodetectors with substantially improved performances [5], [6]. In particular, the ALD coating method makes it possible to tune the MCP capabilities to meet the requirements of different applications [5], [7]. The overall goal of the LAPPD project was to produce commercializable, low-cost 20 cm ×20 cm photodetectors.

The LAPPD collaboration has been very successful in the development of high gain MCPs [8]–[10], large area bialkali photocathodes [11], and waveform sampling electronics [12]. However, the hermetic seal of a large-area detector turned out to be challenging [8]. Given the difficulty in fabricating a 20 cm ×20 cm sealed MCP photodetector, Argonne National Laboratory (ANL) proposed, designed and built a small single tube processing system (SmSTPS) that can produce prototype MCP photodetectors at a reduced size. The SmSTPS maintains an ultra-high vacuum level at 10^{-10} Torr. Currently, ANL is producing all-glass body, small form factor, 6 cm × 6 cm, sealed MCP photodetectors, using MCPs functionalized by ALD [5], [10]. The modular design employs an all-glass enclosure with an indium seal. Design and fabrication of 6 cm × 6 cm photodetectors has been well demonstrated and tested. The SmSTPS has been routinely producing sealed photodetectors at a rate of one device every two weeks.

Two major production runs have been concluded so far. The first production run (07/2014 to 12/2014) adopted the original LAPPD design [4], [13] and produced a number of sealed prototype photodetectors which were characterized using a pulsed blue laser with a wavelength of 405 nm and were shown to have satisfactory performances with a time resolution of about 57 ps for single photoelectrons and spatial resolution of better than 1 mm for large pulses [14], [15].

Manuscript received July 1, 2016; revised October 7, 2016; accepted November 9, 2016. Date of publication November 24, 2016; date of current version July 14, 2017. This work was supported by the U.S. Department of Energy, Office of Science, Office of Basic Energy Sciences and Office of High Energy Physics under Contract DE-AC02-06CH11357. *(Corresponding author: Jingbo Wang.)*

The authors are with High Energy Physics division, Argonne National Laboratory, 9700 South Cass Avenue, Lemont, IL 60439 USA (e-mail: wjingbo@anl.gov; byrum@anl.gov; demarteau@anl.gov; rdharmapalan@anl.gov; jelam@anl.gov; amane@anl.gov; may@anl.gov; rgwcdf@hep.anl.gov; drw@anl.gov; jxie@anl.gov; lxia@anl.gov; hzhao@anl.gov).

Color versions of one or more of the figures in this paper are available online at http://ieeexplore.ieee.org.

Digital Object Identifier 10.1109/TNS.2016.2632748

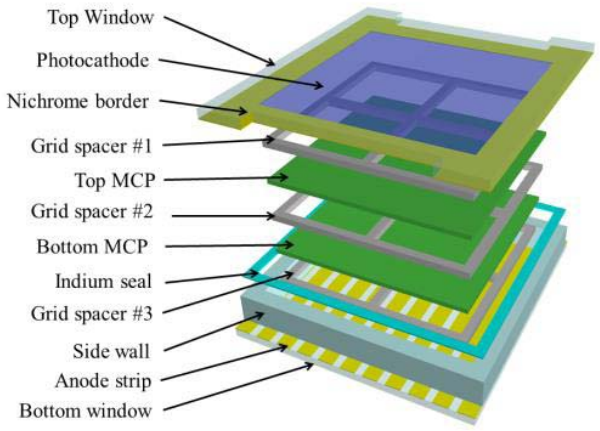

Fig. 1. Basic structure of the 6 cm ×6 cm photodetector with the original LAPPD design [14].

The original LAPPD design required the internal detector components to have matched resistances that are controlled by ALD process. The high voltage (HV) is applied only to the photocathode, and the entire internal stack serves as an internal voltage divider. This design offered a simple solution for biasing the detector, but it was impossible to further optimize the bias voltages for each internal detector component. In order to individually tune the bias voltages for the internal components of the sealed detector, an Independently Biased Design (IBD) of the electrical connection was recently developed and tested. The second production run (06/2015 to 12/2015) has produced 11 sealed devices using the IBD design. Ten devices have shown typical MCP signals under blue laser illumination. Preliminary test results have shown a gain on the order of 10^7 and a time resolution near 35 ps [15]. In this paper, the results of the bias voltage optimization are presented and the performances of the IBD devices are summarized.

II. Sealed Detector Design Improvement

The 6 cm × 6 cm MCP photodetectors that were produced at ANL went through two different designs. The basic schematic structure of the detector is shown in Fig. 1. The sealed detector assembly is comprised of a borosilicate top window, a pair of microchannel plates, three glass grid spacers, a bottom window and a glass side wall.

The side wall is bonded to the bottom glass window, producing the photodetector base. The anode readout strips are printed on the inner surface of the bottom window, extending through the side wall from vacuum to air. A pair of MCPs is made of borosilicate capillary array coated by ALD, featuring 20 μm pores, a length-to-diameter (L/D) ratio of 60 and an open area ratio of about 65%. The MCPs are arranged in a "chevron" configuration (double plates) with 8° pore bias angles. Three grid spacers are located between the top window and the upper MCP, between the two MCPs, and between the lower MCP and the bottom anode plate. A bialkali photocathode is coated in vacuum onto the inner side of the top window. All the package components are made of borosilicate float glass that is considerably less expensive than the leaded glass used in commercial MCPs. The hermetic seal is provided by the top window, the side wall and the bottom window. The side wall is glass-frit bonded to the bottom window. After the photocathode is deposited in vacuum, the top window is sealed with indium to the side wall through a low temperature thermo-compression sealing technique.

In the original LAPPD design, both the MCPs and the grid spacers were ALD-coated with a resistive layer, providing the desired resistances for the internal voltage divider. The MCPs provide multiplication of the photoelectrons, and the spacers provide support from the atmospheric pressure coming from the top and bottom windows. This entire detector can be biased using a single HV connection on the nichrome border of the top window. The MCPs and the spacers serve as a resistor chain, determining the bias voltages for all the components. This design is simple to implement and potentially low cost, featuring no pins which penetrate the hermetic package. In the first production run, a number of prototype photodetectors were successfully fabricated with this initial design. However, processing and testing of these detectors revealed several fundamental issues: 1) this design requires MCPs and grid spacers with specific resistance values, but sometimes it is difficult to find suitably matched parts; 2) during the baking and scrubbing process, the component resistances may change in an uncontrolled way, thereby breaking the resistance match; 3) once a detector is sealed, it is impossible to optimize performance as there is no way to individually control the bias voltages of the detector components; 4) photocathode quantum efficiency (QE) cannot be directly measured as there is no direct electrical contact to the top surface of the upper MCP to collect the emitted photoelectrons.

During the second production run, a new design was developed with minimum modifications to the original LAPPD design [15]. The new design, referred to as IBD, provides connections to all the MCP surfaces. Fig. 2 shows a schematic of the IBD design and Fig. 3 shows a picture of the complete sealed device including the readout board. In this design, only the MCPs are resistive-coated by ALD. The glass grid spacers are insulators without ALD coating, providing support to the sealed photodetector from implosion due to the atmospheric pressure load. A new way to construct the detector package was invented to bring the bias voltage contact from the MCP surface to the outside. To apply a bias voltage to the MCPs, ultra-thin metal shims are attached to the MCP surfaces and aligned with the grid spacers. Each shim has a finger tab that routes the MCP surface contact to an unused silver readout strip on the anode plate. In this way, four additional voltage connections for the MCP biasing can be obtained with very little modification to the existing detector configuration. In the second production run, 11 sealed detectors were fabricated with this improved design. Ten out of eleven were working devices with a production yield of about 91%. This new design for assembly of the MCP photodetector is currently undergoing the patent application process and details will be published elsewhere soon.

As shown in Fig. 2, The IBD design requires five independent electrical contacts from outside the detector into the vacuum, which allows fine tuning of the bias voltage for each

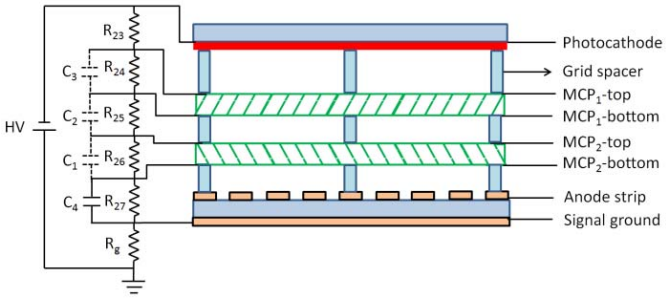

Fig. 2. Electrical circuit diagram of the photodetector with IBD design. The MCPs are coated by ALD, providing the desired resistance. The insulating grid spacers are placed between the top (or bottom) window and the MCP, and between the two MCPs, providing support for the internal stack. Ultra-thin metal grid shims (not shown in this figure) are attached to both the top and bottom surfaces of the MCPs, providing electrical contact for voltage biasing.

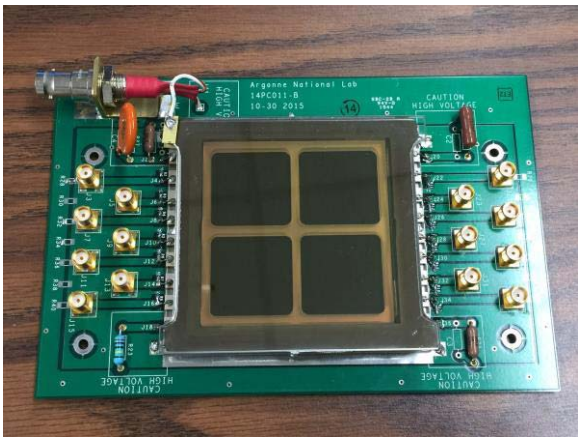

Fig. 3. Picture of a sealed photodetector that is attached to a readout circuit board. Only a single HV is needed to bias the entire detector. The resistors on the readout board are replaceable, offering a simple way to modify the bias voltages of the detector components.

internal detector component. In addition, the photoelectron current can then be directly collected by the top surface of the upper MCP, which enables precise QE measurements. Once the optimal bias voltages are determined, the photodetector is soldered to a readout circuit board that includes a replaceable resistor chain working as an external HV divider, thereby requiring only a single HV connection to the photocathode.

To fabricate the photodetectors, a fabrication system (SmSTPS) [14] was constructed at ANL. The SmSTPS is an ultra-high vacuum transfer system that consists of four independent sub-systems: 1) a vacuum load-lock for loading the detector parts; 2) a bake and scrub chamber for preconditioning; 3) a photocathode deposition chamber for photocathode evaporation; 4) a sealing chamber for making the hermetic seal. The system is equipped with magnetic transfer arms which allow for the transfer of components between the subsystems while operating it from the outside. The entire system is pumped by several turbo molecular pumps and ion pumps, resulting in an ultra-high vacuum level of 10^{-10} Torr that is required for the growth of air-sensitive bialkali photocathodes and photodetector assembly. Photodetector processing recipes are being developed in this

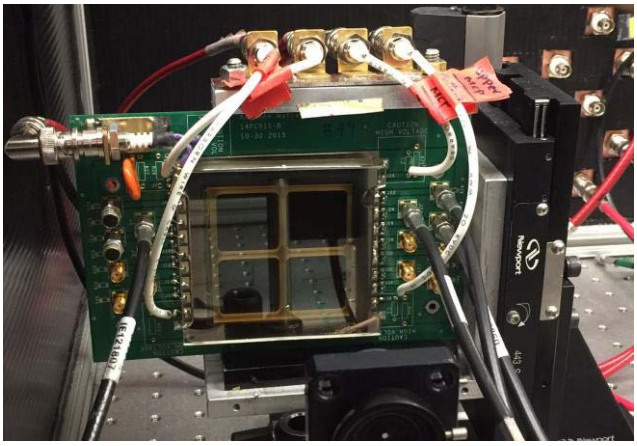

Fig. 4. Sealed photodetector attached to the test stand in the dark box. Detector has five independent HV connections, which allows individually optimizing the bias voltage for each detector component.

system so that the knowledge and experiences can be transferred to industry for the commercialization of large-area (20 cm $\times$ 20 cm) devices. More detailed descriptions of this system can be found in [14], and [15].

III. Test Setup

A blue pulsed laser facility was designed and constructed at ANL for characterizing the MCP photodetectors [14]. The facility can provide a pulsed laser beam with a wavelength of 405 nm and a pulsewidth of 70 ps FWHM. Fig. 4 shows an MCP photodetector on the test stand during bias voltage studies. The test stand is attached to a 2-D translation holder that allows a positional scan in both horizontal and vertical directions.

In order to individually tune the bias voltages of each detector component during operation, the resistors on the readout circuit board are removed and the HVs are directly applied to all the internal stack components using five HV wires. The bias voltages are provided by a programmable multi-channel HV supply.[1] Thus, a remote computer controlled voltage scan is feasible during the laser illumination. For the bias voltage studies and optimization, all five bias voltages are initially fixed to their nominal values based on our previous measurement experiences, and then the voltage is tuned for the component of interest during illumination.

The signals are read out by the anode strips and sent to the circuit board that is printed with traces that have a characteristic impedance of 50 Ω. Unused strips are terminated by 50 Ω resistors on both ends. For data acquisition, the raw waveforms are recorded by a programmable Keysight oscilloscope[2] with a 6 GHz full bandwidth and a maximum 20 Gs/s sampling rate. The data analysis is based on a waveform sampling method, including pulse shape processing, pulse selection and timing discrimination. A detailed description of data analysis can be found in [14].

[1] Wiener MPod mini crate model 037.0001.
[2] Keysight infiniium S-Series model MSO-S 604A.

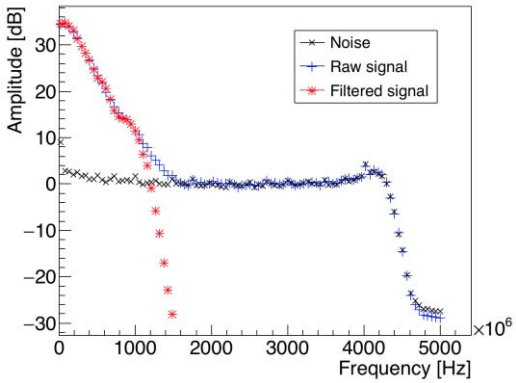

Fig. 5. Average frequency spectrums of the waveform traces. Black: frequency components of the noise obtained with the laser blocked; Blue: frequency components of the raw signals; Red: frequency components of the signals processed by applying a low-pass filter.

IV. Results and Discussion

The QE was measured with a separate optical-electrical system. The bialkali photocathode shows a spectra response in the range from 250 to 600 nm wavelengths, with a peak value of about 14% at 340 nm. The photocathode deposition recipe and the performance characterization are described and discussed in [11].

The light intensity was attenuated by three neutral density filters, and the single photoelectron light level was statistically reached when less than 10% of the laser pulses produce a valid signal in the photodetector [14]. In this paper, the tests for the bias voltage optimization were done at single photoelectron light intensity, which was completely independent of the photocathode QE.

To study the bias voltage dependence for the photodetectors, the voltages of the detector components were initially set to nominal values: 300 V between the photocathode and the upper MCP; 900 V across the MCP; 300 V between the two MCPs; 400 V between the lower MCP and the anode.

A. Typical Signals

The raw signal waveforms are recorded by a four-channel Keysight oscilloscope with a sampling rate of 10 Gs/s for each channel. The frequency components of the raw waveforms are analyzed by the fast Fourier transform (FFT) algorithm. The frequency spectrums of the noise, the raw signals and filtered signals were analyzed and the average spectrums are shown in Fig. 5. In the frequency domain, the signal is well distinguished from the noise up to about 1.5 GHz, which allows the application of a low-pass filter to suppress the high frequency noise. A typical Butterworth filter is applied with a cutoff frequency at 1.3 GHz. Then, the filtered frequency spectrum is converted to the time-domain waveform through an inverse FFT transform. The oscilloscope is capable of 6 GHz full bandwidth if less than two of the four input channels are used. In this measurement, three were used, which allows an operating bandwidth of 4.2 GHz. In Fig. 5, the sudden drop between 4–5 GHz is related to the bandwidth limitation of the oscilloscope. The frequency filtering algorithm leads to an improvement of the pulse quality and the time resolution. Typically, the impact is dependent on the signal-to-noise ratio. The filtering has a high impact in low gain operations, while it plays a less important role in high gain operations.

Fig. 6 shows the raw and filtered signal waveforms at different bias voltages across the MCP, obtained at single photoelectron light level. The raw and filtered signals obtained at a MCP voltage of 860 V are shown in Fig. 6(a) and (b), respectively. The average gain is on the order of 10^7, providing an excellent signal-to-noise ratio. There is little difference between the raw and the filtered waveforms, which indicates that the frequency filtering has a small impact. The same result is shown in Fig. 6(c) and (d) for MCP voltage of 760 V. As the pulse height is much smaller, the noise level becomes a noticeable factor that can affect waveform shape. In this case, the frequency filtering is essential to suppress the noise and improve the waveform quality. The signals of the IBD photodetectors have a 3–4 ns pulsewidth over a threshold that is 10% of the pulse height. The rise time is about 600 ps, determined by the geometry and the bias voltages across the detector components.

B. Gain Distribution

The MCPs of the photodetectors are made of a borosilicate glass substrate that is ALD coated with a resistive layer and a secondary electron emissive (SEE) layer. MgO is used as the emissive material and the deposition parameters are optimized for secondary electron emission. To measure the gain, the laser light intensity was attenuated to the single photoelectron level as defined in [14]. Fig. 7 shows the gain distribution of an IBD photodetector. The gain distribution features a high pedestal at zero and a single photoelectron peak. The pulse selection is performed using a time over threshold (TOT) cut. The root mean square (RMS) is calculated for the amplitude of the waveform baseline and the threshold is set to five times the RMS. This calculation is performed event by event, so each waveform has its own threshold. A valid pulse is defined as a waveform having a duration that is more than 500 ps over the threshold. The average gain of the pulses that pass the quality cut is higher than 10^7. There is a clear valley between the pedestal and the single photoelectron peak, indicating a good signal-to-noise ratio.

C. Timing Response

The 405-nm blue pulsed laser has a pulse duration of 70 ps FWHM ($\sigma \sim 30$ ps), which allows timing measurement of the MCP photodetectors. The measurements were done at single photoelectron light intensity. The photon transit time is defined as the delay between the input laser synchronization pulse and the output MCP photodetector signal. The incident photons are converted to photoelectrons by the photocathode. The photoelectrons are multiplied by the MCPs and the electron cloud is collected by the anode striplines. The time is measured by both sides of the same stripline, and the average time is taken as the arrival time of the MCP photodetector. The transit time of the photons differs, depending on each electron multiplication process. The distribution of the transit time is

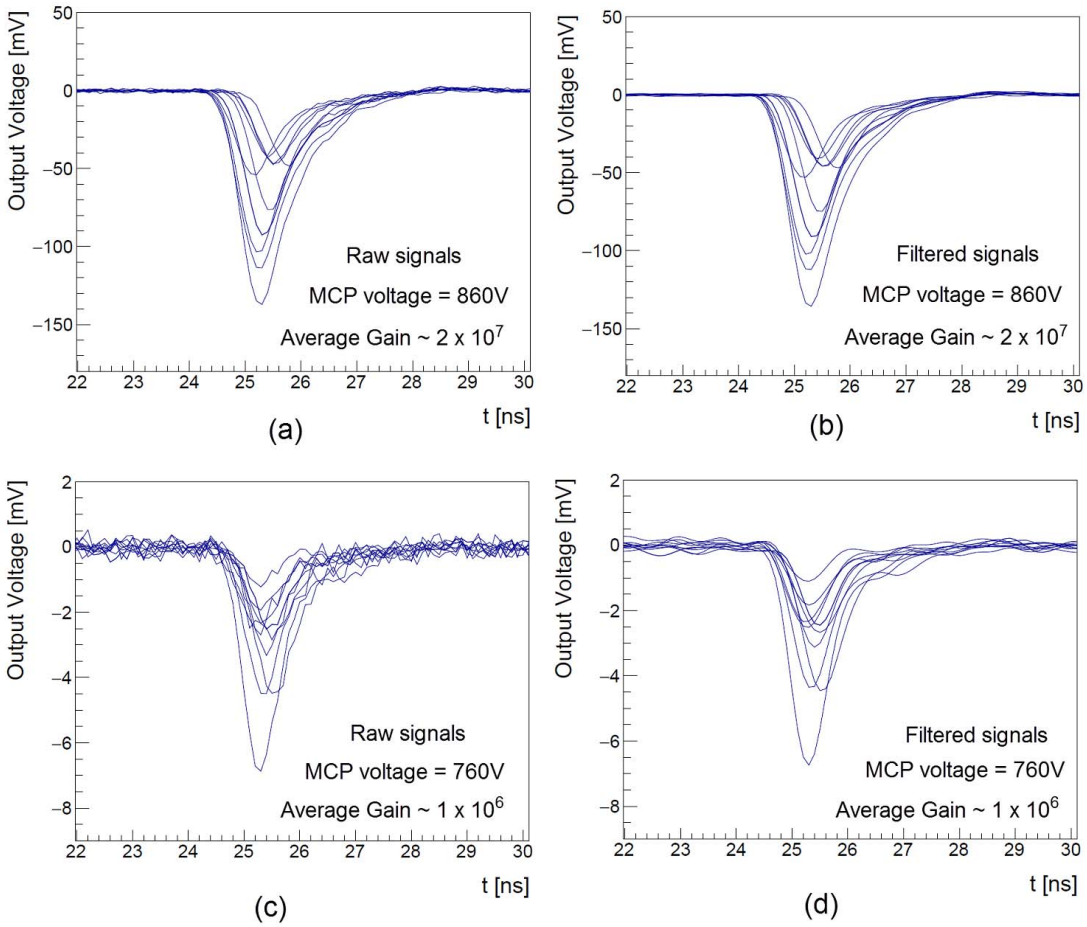

Fig. 6. Typical signals of the IBD photodetectors: (a): raw signals at an MCP bias voltage of 860 V; (b) filtered signals at an MCP bias voltage of 860 V; (c) raw signals at an MCP bias voltage of 760 V; and (d) filtered signals at an MCP bias voltage of 760 V.

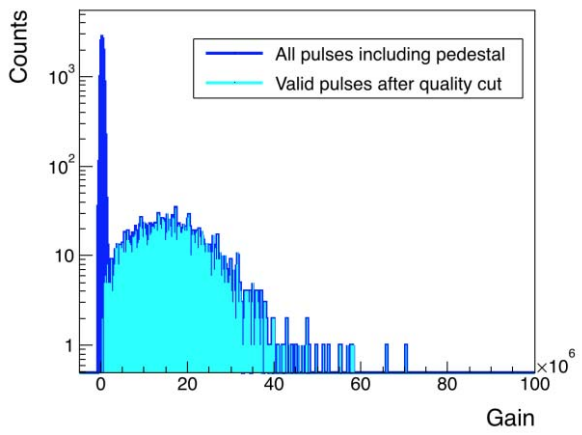

Fig. 7. Gain distribution of the IBD device.

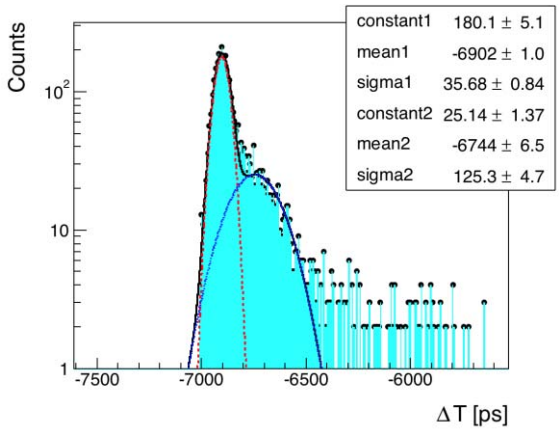

Fig. 8. Transit time distribution for single photoelectrons.

defined as the transit time spread (TTS). The system measures the overall time resolution which includes the laser jitter, the intrinsic TTS of the MCP photodetector and the resolution of the readout electronics.

The typical distribution of the transit time obtained at nominal bias voltages is shown in Fig. 8. This distribution features a main prompt peak followed by a long tail. The first peak represents the timing of the photoelectrons that get into the MCP pore and instantly initiates an electron avalanche. When the photoelectrons hit the solid surface of the MCP top surface or the exposed region of the MCP pores, they may get backscattered towards the photocathode. The backscattered photoelectrons are then pulled back by the electrical field into the MCP pores at a different position and form an electron

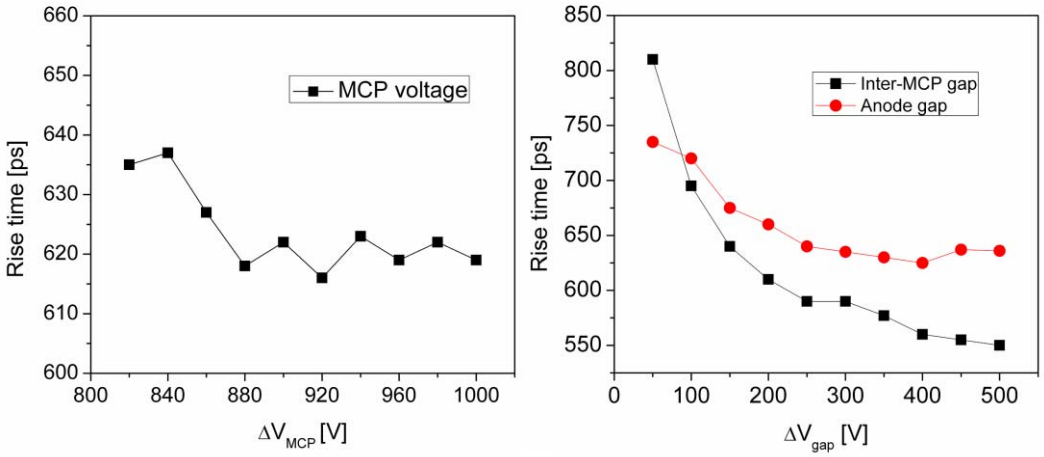

Fig. 9. Rise time versus bias voltages. Left: rise time as a function of the voltage across the MCP; right: rise time as a function of the inter-MCP gap voltage (black) and the anode gap voltage (red).

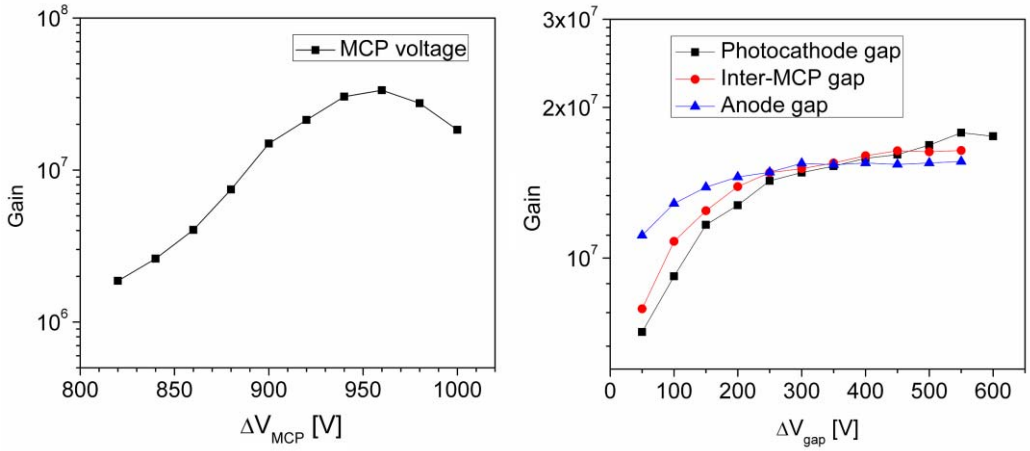

Fig. 10. Gain versus bias voltages. Left: gain as a function of the voltage across the MCP; right: gain as a function of the photocathode gap voltage (black), the inter-MCP gap voltage (red) and the anode gap voltage (blue).

avalanche that is delayed by a few hundred picoseconds. In Fig. 8, a double-Gaussian fit was applied to the transit time distribution. The standard deviation of the first Gaussian is used to estimate the overall time resolution, and the second Gaussian is attributed to the backscattered electrons. The laser pulse may have an intrinsic timing structure within its duration. Although the second Gaussian in the timing distribution is most likely attributed to the electron backscattering, there might be a contribution from the laser intrinsic timing structure. The intrinsic laser structure can be precisely measured in the future by a streak camera that has better than 1-ps time resolution.

D. Bias Voltage Optimization

The performances of the photodetectors were found to be dependent on the bias voltages across the photocathode gap, the MCPs, the inter-MCP gap and the anode gap. To measure the bias voltage dependence for each component, only the one voltage of interest was changed and the other voltages were kept at the nominal values during the test. This process was performed for all the components individually, and the optimized voltages were experimentally determined.

The rise time of a pulse is traditionally defined as the time taken for a signal to change from 10% to 90% of the pulse height. In an MCP photodetector, the rise time is affected by the detector geometry, the bias voltage and the electron avalanche statistics. In the photocathode gap, the emitting photoelectrons have a negligible initial energy of a few electron volts. In addition, there is no electron multiplication. As a consequence, the signal produced by a single photoelectron that drifts in the photocathode gap is too small to be detected, not exceeding electronics noise level. Therefore, the bias voltage across the photocathode gap does not affect the rise time. The signal rise time is studied as a function of the MCP voltage, the inter-MCP gap voltage, and the anode gap voltage. The test results are shown in Fig. 9. With the increase of the bias voltages, the rise time improves rapidly at first and eventually tends to reach a stable value.

The gain and the time resolution are scanned as a function of the MCP voltage, the photocathode gap voltage, the inter-MCP

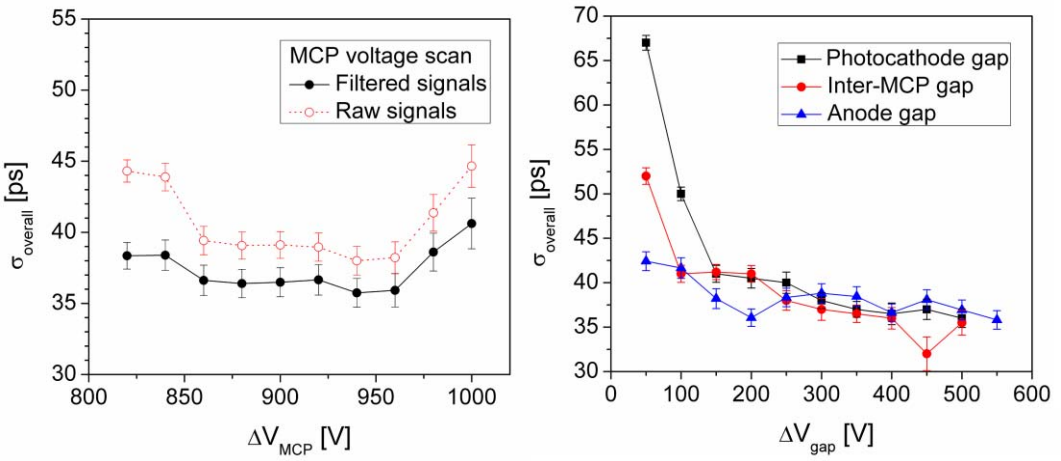

Fig. 11. Overall time resolution versus bias voltages. Left: time resolution as a function of the voltage across the MCP; right: time resolution as a function of the photocathode gap voltage (black square), the inter-MCP gap voltage (red circle) and the anode gap voltage (blue triangle).

gap voltage and the anode gap voltage. The result of the gain measurement is shown in Fig. 10 and the result of the corresponding time resolution measurement is shown in Fig. 11.

For an MCP photodetector, the dominant factor of the time resolution is the electron avalanche statistics inside the MCP pores. As shown in Fig. 11 (left), the gain and the time resolution initially improve with increasing MCP bias voltage, but deteriorate when the bias voltage is higher than 950 V. This effect may be related to the gain saturation and a slow discharge in the pores. Generally, the gain increases with the voltage and eventually gets saturated. However, when the voltage is too high, a slow discharge is observed using the oscilloscope in self-triggering mode, featuring a negative polarity, a few hundred mV pulse height and a few μs pulse duration. The discharge is not initiated by the photons but something else inside the vacuum package. The possible reasons include instability of the MCP at a huge gain, consecutive ion feedback, field electron emission and residue gas breakdown between close components. The mechanism of the described discharge is still unclear and future studies are needed to explain this observation. The discharge pulse produces a huge drain current along the MCP pores and exhausts the secondary electron emissive layer. When the slow discharge appears, the gain drops and the time resolution deteriorates. The time resolutions before and after frequency filtering are shown in Fig. 11 (left). At low MCP voltages, frequency filtering improvement is about 7 ps, indicating a good enhancement of the signal-to-noise ratio. The improvement at MCP voltages higher than 860 V is typically less than 4 ps thanks to the high gain.

The voltages across the photocathode gap and the inter-MCP gap are also important to the time resolution. The electrons released from the photocathode and the MCP pores have a low energy of a few electron-volts. The bias voltages across the photocathode and the inter-MCP gaps are used to accelerate the low-energy electrons. According to our previous measurement of the SEE layer, the electron needs to have an energy of higher than 60 eV to release more than two secondary electrons from the MgO emissive layer [6]. The number of the secondary electrons produced by the first few strikes dominates the final detector gain and time resolution. The measured time resolution as a function of these voltages is shown in Fig. 11 (right).

Based on the bias voltage scans for each detector component, we came up with an optimized bias voltage setting that is also referred to as the nominal bias voltages. It has to be noted that the photocathode lifetime is not taken into account for the selection of the nominal bias voltages. At the typical MCP voltage, the gain is extremely high. During the electron avalanche evolution, the residual gas or the absorbed atoms on the MCP wall surface can be ionized by the electrons. These ions are then accelerated by the electrical field and drift towards the photocathode. If the ions gain sufficient energy, they can release electrons from the photocathode or the MCP wall, which initiates a second electron avalanche that is referred to as the after pulse. The after pulses at the level of 8% were observed at the nominal voltages, which may lead to a deterioration of the photocathode lifetime. For applications that require a long photocathode lifetime, the MCP photodetectors need to be operated at lower voltage. A systematic study on the ion feedback will be done soon.

E. Performance of the IBD Devices

The measurements of the gain and time resolution were performed for eight IBD devices at different bias voltages. The relation between the overall time resolution and the gain is shown in Fig. 12. It was found that the gain and the time resolution were strongly affected by the appearance of slow discharges at very high voltages. The abnormal data points due to these slow discharges at extremely high bias voltage are omitted from the figure. Although further studies of these slow discharges are forthcoming, we believe they are most likely attributed to the production process and not related to the intrinsic time resolution. Under normal working condition, the gain reaches the order of 10^7. The overall time

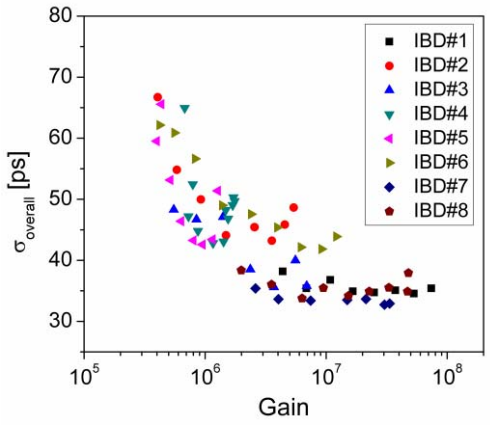

Fig. 12. Relation between the overall time resolution and the gain, obtained from eight IBD devices.

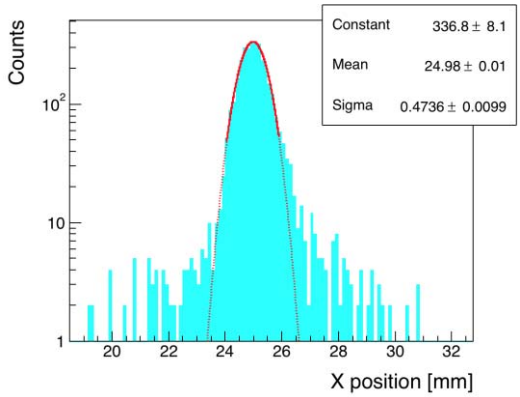

Fig. 13. Photon position distribution along the readout strip. The solid line corresponds to a Gaussian curve within $\pm 2\sigma$ range.

resolution is about 35 ps, including the jitter of the laser pulse (FWHM = 70 ps). To estimate the TTS, the laser jitter is usually subtracted from the measured overall time resolution. Given that the laser pulse duration is comparable to the overall time resolution, this subtraction has not been made. The laser may have an intrinsic timing structure within the pulse duration. The analysis of time resolution might include part of the laser jitter that is less than 30 ps sigma, so an arbitrary subtraction may lead to an overestimate of the TTS. The overall time resolution shown in Fig. 12 is a convolution of the TTS, the laser contribution and the electronics contribution, which gives an upper limit on the TTS. A faster laser is needed to precisely measure the TTS.

Typically, the time resolution improves with the increase of the gain. However, as shown in Fig. 12, sometimes the time resolution starts to deteriorate with the gain increasing. This behavior is usually observed from the photodetectors that are made with low gain or noisy MCPs. The gain increase as one raises the HV across the MCP. However, the dark noise level increases accordingly at the same time which in return degrades the time resolution. In principle, it is not recommended to operate the reported MCP photodetectors at voltages with the appearance of the time resolution deterioration. All the photodetectors presented in this paper have MCP pores with a 20 μm diameter. The time resolution is expected to be further improved if MCPs with smaller pore size are used.

As the gain is huge, no front end electronics are needed to amplify the signal, which simplifies the detector design and saves on cost. It has to be noted that the gain of sealed photodetectors varies from 10^5 to 10^8, depending on the quality of the MCP samples. In addition, the final gain was found to depend on the detector processing inside the fabrication system, such as the baking and scrubbing. At the moment, we are improving the detector processing parameters, aiming at a good control of the MCP properties and the stabilization of the detector performances.

Fig. 13 shows the photon position distribution along the readout strip. Given the signal transmission speed of about 0.2 mm/ps in the strip, the photon position is calculated by the time difference between two strip ends. With the optimized voltages, the signal-to-noise ratio is significantly improved, resulting in a spatial resolution of about 0.5 mm. This result is much better than that of the photodetectors with the first design [14].

V. Conclusion

ANL is currently producing all-glass body, 6 cm $\times$6 cm, permanently sealed photodetectors, using MCPs functionalized by ALD. Design improvement and bias voltage optimization of the photodetectors are described in this paper. In order to optimize the performance of the photodetectors, the original LAPPD design was modified and an IBD design was recently developed and tested. A series of sealed photodetectors with the IBD design were produced and characterized. The bias voltage was studied and optimized for each internal detector component and the performance was measured with a pulsed laser. Using the optimized voltages, the IBD devices have shown a gain on the order of 10^7, a time resolution of better than 35 ps, and a spatial resolution of better than 1 mm.

Acknowledgment

This work would not have been possible without the dedicated efforts of the LAPPD collaboration. The authors would like to thank H. Frisch (University of Chicago) for the initial design of the LAPPD detectors. They are grateful to Incom., Inc., for providing the excellent MCP substrates. They thank R. Kmak (ANL) for the design of the vacuum chamber, as well as J. Gregar (ANL) of the glass shop, for his talented work on the frit seal. They are grateful to G. Drake (ANL), T. Cundiff (ANL) and F. Skrzecz (ANL) for help with the electronic and the mechanical designs.

References

[1] Hamamatsu. *Photomultiplier Tubes, Basics and Applications*. [Online]. Available: https://www.hamamatsu.com/resources/pdf/etd/PMT_handbook_v3aE.pdf

[2] M. Demarteau *et al.* (2014). " Planning the future of U.S. particle physics (Snowmass 2013): Chapter 8: Instrumentation frontier." [Online]. Available: https://arxiv.org/abs/1401.6116

[3] J. L. Wiza, "Microchannel plate detectors," *Nucl. Instrum. Methods*, vol. 162, nos. 1–3, pp. 587–601, 1979.

[4] *The LAPPD Collaboration*. [Online]. Available: http://psec.uchicago.edu
[5] A. U. Mane *et al.*, "Atomic layer deposition of nanostructured tunable resistance coatings: Growth, characterization, and electrical properties," *ECS Trans.*, vol. 64, no. 9, pp. 3–14, 2014.
[6] S. Jokela *et al.*, "Secondary electron yield of emissive materials for large-area micro-channel plate detectors: Surface composition and film thickness dependencies," *Phys. Procedia*, vol. 37, pp. 740–747, 2012.
[7] R. Dharmapalan *et al.*, "MCP-based photodetectors for cryogenic applications," *J. Instrum.*, vol. 11, no. 2, p. C02019, Feb. 2016.
[8] O. H. W. Siegmund *et al.*, "20 cm sealed tube photon counting detectors with novel microchannel plates for imaging and timing applications," *Phys. Procedia*, vol. 37, pp. 803–810, 2012.
[9] M. J. Minot *et al.*, "Pilot production & commercialization of LAPPD," *Nucl. Instrum. Methods Phys. Res. A, Accel. Spectrom. Detect. Assoc. Equip.*, vol. 787, pp. 78–84, 2015.
[10] A. U. Mane and J. W. Elam, "Atomic layer deposition of W:Al_2O_3 nanocomposite films with tunable resistivity," *Chem. Vapor Deposition*, vol. 19, nos. 4–6, pp. 186–193, 2013.
[11] J. Xie *et al.*, "Instrumentation for theory-inspired photocathode development within the large area picosecond photodetector (LAPPD) project," *Phys. Procedia*, vol. 37, pp. 811–819, 2012.
[12] E. Oberla, J. F. Genat, H. Grabas, H. Frisch, K. Nishimura, and G. Varner, "A 15 GSa/s, 1.5 GHz bandwidth waveform digitizing ASIC," *Nucl. Instrum. Methods Phys. Res. A, Accel. Spectrom. Detect. Assoc. Equip.*, vol. 735, pp. 452–461, Jan. 2014.
[13] B. Adams *et al.*, "An internal ALD-based high voltage divider and signal circuit for MCP-based photodetectors," *Nucl. Instrum. Methods Phys. Res. A, Accel. Spectrom. Detect. Assoc. Equip.*, vol. 780, pp. 107–113, Apr. 2015.
[14] J. Wang *et al.*, "Development and testing of cost-effective, 6 cm×6 cm MCP-based photodetectors for fast timing applications," *Nucl. Instrum. Methods Phys. Res. A, Accel. Spectrom. Detect. Assoc. Equip.*, vol. 804, pp. 84–93, Dec. 2015.
[15] J. Xie *et al.*, "Design and fabrication of prototype 6 × 6cm^2 microchannel plate photodetector with bialkali photocathode for fast timing applications," *Nucl. Instrum. Methods Phys. Res. A, Accel. Spectrom. Detect. Assoc. Equip.*, vol. 784, pp. 242–247, Jun. 2015.
[16] J. Wang *et al.*, "Recent progress in the development of 6 cm×6 cm micro-channel plate based photodetectors at Argonne National Laboratory," in *Proc. IEEE NSS/MIC*, San Diego, CA, USA, Oct./Nov. 2015, pp. 1–5.